The Pyrolytic Reaction of Ketonic Hydrazones from *S*-Methyl Dithiocarbazate: A Combined Online GC-MS Pyrolysis and DFT Study

Kezhi Jiang,[†,‡] Gaofeng Bian,[‡] Huayu Qiu,[‡] Yuanjiang Pan,*[,†] and Guoqiao Lai*[,‡]

Department of Chemistry, Zhejiang University, Hangzhou, 310036, China, and Key Laboratory of Organosilicon Chemistry and Material Technology, Hangzhou Normal University, Hangzhou, 310012, China

Received: April 15, 2008; Revised Manuscript Received: November 11, 2008

The gas-phase pyrolysis of ketonic hydrazones from *S*-methyl dithiocarbazate $R^1R^2C{=}N{-}NHC(=S)SCH_3$ (R^1, R^2 = alkyl or aryl) was investigated by online GC-MS pyrolysis and theoretical calculation. Both of these pyrolytic products, ascribed to methanethiol and the corresponding *N*-isothiocyanate imines, were detected in the total ion chromatography (TIC) of GC-MS. Calculation results exhibit two stable configurational structures for reactants (Re), which can interconvert with relatively low barriers (<78 kJ/mol). DFT calculations showed that the two unimolecular pyrolytic processes, a direct 1,2-elimination of CH_3SH for *syn*-Re and a two-step reaction pathway for *trans*-Re involving tautomer interconversion followed by decomposition of CH_3SH, are competitive in the reaction. Both ***syn*-Re** and ***trans*-Re** exhibit lower critical energies in the propagation step of the radical pyrolysis than that in the unimolecular pyrolysis process (187.76 kJ/mol via 131.91 kJ/mol for ***syn*-Re**, and 159.15 kJ/mol via 98.92 kJ/mol for ***trans*-Re**). However, much more energy is needed to excite the compound to produce the methylthio radical, with 262.03 and 253.60 kJ/mol for ***syn*-Re** and ***trans*-Re**, respectively. Therefore, the unimolecular pyrolysis rather than the radical one occurs in the condition of this study.

Introduction

Compounds undergo pyrolysis with no other reagent present when heated,[1] which had been developed as an analytical technique to obtain the structural information of polymers.[2] Also, the pyrolysis of thermally unstable micromolecules in the injector of GC has caught the attention of analysts.[3] Study on the pyrolytic behavior of micromolecule and speculation on the mechanism of the reaction might be helpful in its GC quantitative determination[3] and the structural analysis of the relative polymers.[2] One type of pyrolyisis mechanism involves unimolecular gas-phase elimination through a cyclic transition state,[1] such as pyrolysis of carboxylates,[4] xanthates,[5] amine oxides,[6] phosphate esters,[7] β-hydroxy alkenes,[8] etc. The second one involves free radical reaction,[1] which occurs in pyrolysis of halides,[9] alkanethiols,[10] and certain carboxylic esters.[11]

Derivatives of thioureas were also reported to undergo pyrolytic reaction with no definite reaction mechanism. Pyrolysis of the dithiocarbamic amide of primary amines and *N*-allyl-*N*′-arylthious was reported to occur in the heated GC injector and gave rise to the corresponding isothiocyanates.[3] However, we found that pyrolysis of *S*-methyl arylmethylidenehydrazine dithiocarboxylate in the heated GC injector yielded HNCS, CH_3SH, and the corresponding aromatic cyanate, and postulated a six-member cyclic transition state mechanism.[12] Flash vacuum pyrolysis of *N*-alkoxy thioureas was reported to yield alkoyl isothiocyanates.[13] Thermal elimination of 1-furoyl-3-phenylthioureas led to furamide and furoyl isothiocyanate probably through a four-membered cyclic transition state.[14] Pyrolysis of 1,4-diarylthiosemicarbazides in a sealed tube at 200 °C was reported to give NH_3, H_2S, aryl isothiocyanate, aryl amine, diarythiocarbbanilide, benzimidazole derivatives, azobenzene, aryl cyanamide, and phenyl hydrazine, and a free radical mechanism was suggested to account for the pyrolysis.[15] Therefore, it is very significative to further investigate the pyrolytic mechanism of the derivatives of thioureas due to their uncertain reaction mechanisms.

An experimental study was generally carried out in a static system to obtain the kinetic parameters and speculate the mechanism of the reaction.[16] And theoretical calculation has been a powerful tool for investigating the mechanism of reactions so far, to obtain many molecular properties of the relevant species, transition states, and reaction pathways, and the thermodynamic and kinetic parameters.[17]

Lee and co-workers[18] studied the thermal decomposition of alkanoic esters, $Y{=}C(R){-}X{-}CH_2CH_3$ (where X = Y = O or S) by the semiempirical method MO, and found that the decomposition, conforming to a concerted process of the retro-ene reaction, proceeds through a six-membered cyclic transition state. Carcía and co-workers[19] have studied the water-catalyzed decomposition of dithiocarbamates with the DFT method. They found that *N*-methyl dithiocarbamic acid decomposes via proton transfer assisted by a water molecule, leading to a zwitterionic intermediate followed by a fast N−C bond-breaking process, whereas decomposition of *N*-phenyldithiocarbamic acid occurs through a proton transfer step concerted with the N−C bond-breaking. Ding and co-workers[20] investigated decomposition of the ground state *S*-methyl thioacetate and found that the experimentally dominant process to CH_3SH and H_2CCO is the most dynamically favorable. However, no theoretical study on the thermal decomposition of derivatives of thioureas has been reported to our knowledge.

Hydrazones from *S*-methyl dithiocarbazate are important intermediates used in drug synthesis[21] and also show particular biological activities, such as antibacterial and anticancer.[22] We have found that ketonic hydrazones from *S*-methyl dithiocar-

* Corresponding authors. Y.P.: e-mail yuanjianpang@zju.edu.cn. G.L.: e-mail gqlai@hznu.edu.cn.
† Zhejiang University.
‡ Hangzhou Normal University.

10.1021/jp808273m CCC: $40.75
Published on Web 01/08/2009

CHART 1: The Structures of Compounds 1−5 of the Ketonic Hydrazones from *S*-Methyl Dithiocarbazate

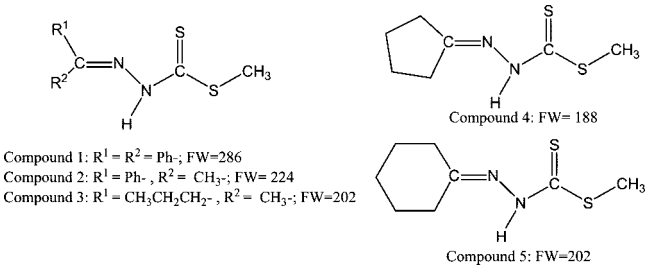

bazate undergo pyrolysis in the heated GC injector, and yield different pyrolytic products from those of aldehyde hydrazones from *S*-methyl dithiocarbazate.[12] In this work, the online pyrolysis of ketonic hydrazones from *S*-methyl dithiocarbazate has been performed on GC-MS, and both the unimolecular and the free radical mechanisms of the process have been studied in detail by using the density functional theory method.

Experimental Procedures

All of the ketonic hydrazones from *S*-methyl dithiocarbazate $R^1R^2C{=}N{-}NH{-}C(=S)\ SCH_3$ (R^1, R^2 = alkyl or aryl) (Chart 1) for study were synthesized according to Scheme 1, purified by washing with *i*-PrOH and recrystallization from CH_2Cl_2 in our laboratory, and later identified by MS and NMR.[12,21]

All the online prolysis experiments were carried out on a Trace 2000 GC/DSQ MS instrument (ThermoFisher Company, USA), equipped with an HP-5 ms capillary column (30 m × 0.25 mm × 0.25 μm, Agilent) and NIST (V2.0) MS spectra library. Control of GC-MS measurements and data acquisition and processing were performed by using Xcalibur software (Version 1.4). Typical parameters were used for the operation of the GC and MS as follows:[23]

A direct introduction MS analysis was preformed by obtaining a trace sample (μg) in a cap in the front of the direct probe, inserting the probe into the ion source (EI), and heating up the cap at a temperature of 150 °C, which was controlled by the direct probe controller (Thermofisher Company, USA), to vaporize the sample directly into the ion source chamber for ionization. Mass analysis was carried out under normal conditions, with the ion source temperature at 200 °C, electron energy at 70 eV, scan rate at 2 s^{-1}, and mass scan range of 35−500 daltons.

GC-MS analysis was performed by using the programmed temperature method as follows: 50 °C → 1 min → 15 deg min^{-1} → 260 °C → 10 min. Unless otherwise stated, the other GC conditions were set as follows: the injector and the X-line temperatures were set at 260 °C and carrier gas (helium gas, 99.999%) was set at the constant flow of 1.0 mL/min. The mass analysis conditions were similar to the above except for mass data acquisition of fragments (0−1.50 min and 2.00−20.00 min). Sample was directly dissolved in CH_2Cl_2 to form weak solution; 0.5 μL of the solution was injected into the injector of GC-MS for analysis.

Computational Details

The theoretical calculations were performed with the Gaussian 03 program.[24] The equilibrium geometries of reactants, transition states, intermediates, and products were optimized by using the density functional theory (DFT) method at the B3LYP/6-31++g(2d,p) level for the unimolecular process and at the uB3LYP/6-31++g(2d,p) level for the radical process, with calculated force constants. No symmetry constraints was imposed in the optimization. All reactants, intermediates, and products were identified as true minima by the absence of imaginary frequencies. Transition states (TS) on the other hand were identified by the presence of one single imaginary vibration frequency with the normal vibrational mode. In addition, transition states were confirmed by the intrinsic reaction coordinates (IRC) calculations. Vibrational frequencies and zero-point energies (ZPE) for all the key species were calculated at the same level of theory. Scaled frequencies were not considered since the errors on the calculated thermodynamical properties are almost negligible at this theoretical level.[25]

Unless otherwise stated, only Gibbs free energies (including thermal correction at 25 °C) were used for the discussion of the relative stabilities of the chemical structures considered.

Hard data on geometries, electronic energies, as well as entropies and Gibbs free energies (at 25 °C) of all structures considered are available as Supporting Information.

Results and Discussion

A. The Online GC-MS Pyrolysis of $R^1R^2C{=}N{-}NH{-}C(=S)SCH_3$. Figure 1 gives the EI-MS of compound **5** (in Chart 1) by the direct introduction method, showing the abundant molecular ion peak at *m*/*z* 202. Decomposition of the molecular ion gives the characteristic fragment ions at *m*/*z* 173, 159, and 155 by losing the radical of $CH_3CH_2^{\bullet}$, $CH_3CH_2CH_2^{\bullet}$, and $CH_3S^{\bullet}$, respectively. Figure 2 shows the TIC of compound **5**, which was performed by GC-MS. Three peaks are found in the TIC of the compound. The peak t_R 1.45 min and the peak t_R 2.09 min are ascribed to methanethiol (CH_3SH) and the CH_2Cl_2 residue reagent by searching its mass spectrum in the NIST02 MS spectra library. The peak t_R 7.97 min shows the molecular ion peak at *m*/*z* 154 (Figure 3) and is attributed to *N*-isothiocyanate cyclohexanimine $(CH_2)_5C{=}N{-}N{=}C{=}S$.

However, no peak with the molecular ion peak at *m*/*z* 202 is found in the TIC of compound **5** (Figure 2). It is interesting to note that the molecular weight of compound **5** (202 daltons) was equal to the sum of the molecular weight of the peak t_R 1.45 min (CH_3SH, 48 daltons) and that of the peak t_R 7.97 min ($(CH_2)_5C{=}N{-}N{=}C{=}S$, 154 daltons) in the TIC. Therefore, we may conclude that compound **5** underwent pyrolysis in the heated injector and yielded *N*-isothiocyanate cyclohexanimine and methanethiol, when analyzed by GC-MS. With direct sample introduction into the ion source in high vacuum condition and at relatively low temperature, the compound rapidly evaporated and ionized to form the abundant molecular ion at *m*/*z* 202 before its decomposition. The peak at *m*/*z* 154 with relative abundance of 8% in the EI-MS (Figure 1) indicates the slight pyrolysis in this process.

The other four compounds in Chart 1 gave similar results in both the direct sample introduction EI-MS and the GC-MS experiments (see Figure S1 and Figure S2 in the Supporting Information). Detailed results are summarized in Table 1. EI mass spectra of compounds **1**−**5**, with abundant molecular ion, can be obtained only by the direct introduction method, whereas they will undergo online pyrolysis when analyzed by GC-MS and give CH_3SH and the corresponding *N*-isothiocyanate imines.

Among the compounds in Chart 1, the R^1 and R^2 groups can be aliphatic or aryl groups, and even cyclic groups for compounds **4** and **5**. The above results clearly indicate that ketonic hydrazones from *S*-methyl dithiocarbazate can undergo online gas-phase pyrolysis to yield methanethiol and the corresponding *N*-isothiocyanate imines. This pyrolytic process is similar to the reported pyrolysis of derivatives of thioureas,

SCHEME 1: The Synthetic Route of the Ketonic Hydrazones from *S*-Methyl Dithiocarbazate

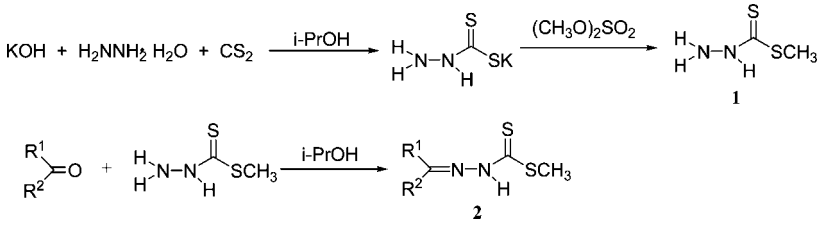

where only the isothiocyanate product was detected in these papers.[3,13] Both of the pyrolytic products have been detected in the TIC in this work, showing that the online GC-MS pyrolysis is a powerful method for the study of pyrolytic reactions.

B. The Effect of the GC Injector Temperature on the Pyrolysis. To further investigate the effect of temperature on the decomposition, a series of online pyrolytic experiments were carried out for compound **5** by reducing the GC injector temperature every 10 °C from 250 to 190 °C. All of the TIC are listed together in Figure 4, where peak t_R 1.46 min, peak t_R 2.09 min, and peak t_R 7.96 min are attributed to methanethiol, the residue solvent CH_2Cl_2, and *N*-isothiocyanate cyclohexanimine, respectively.

It can be also noticed in Figure 4 that the peak t_R 9.39 min appears and rises gradually with a reduction in the GC injector temperature, which gives a similar mass spectrum to the peak t_R 7.97 min with the molecular ion at *m*/*z* 154 (see Figure S3 in the Supporting Information). The peak t_R 7.97 min is very sharp and attributed to the pyrolytic compound (*N*-isothiocyanate cyclohexanimine), which is formed rapidly by decomposition of compound **5** in the heated GC injector. The unreacted compound **5** vaporizes into the capillary column, and continues to decompose when the oven temperature increases slowly by running the programmed temperature method. The peak t_R 9.38 min is confirmed to be the same pyrolytic compound that formed gradually in the capillary column, and exhibits a broad peak in the TIC. That is, pyrolysis of compound **5** is found to occur in both the injector and the capillary column of the GC-MS when the GC injector is set at a relatively low temperature.

TABLE 1: The Mass Spectra Data and GC-MS Data of Ketonic Hydrazones from S-Methyl Dithiocarbazate

compounds	molecular ion (by direct introduction MS) (*m*/*z*)	molecular ion of main peaks in TIC (by GC-MS) (t_R, *m*/*z*) no. 1	no. 2
1	286		t_R 14.47 min, 238
2	224		t_R 11.22 min, 176
3	204	t_R 1.45min, 48 (CH_3SH)	t_R 6.84, 7.04 min, 156
4	188		ˆ t_R 8.60 min, 140
5	202		t_R 7.97 min, 154

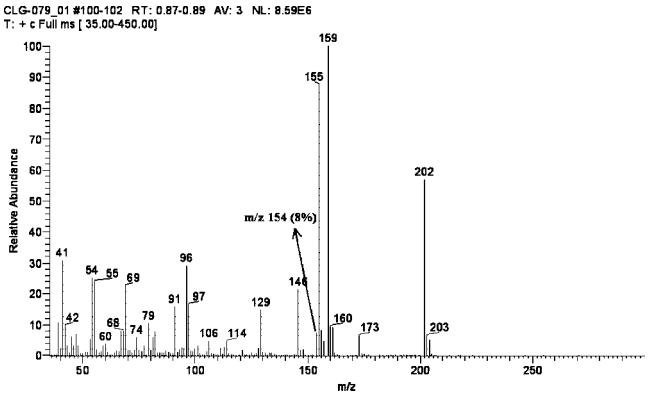

Figure 1. Mass spectrum of $(CH_2)5C{=}N{-}NHC(=S)SCH_3$ compound **5** by direct introduction, with the molecular ion at *m*/*z* 202.

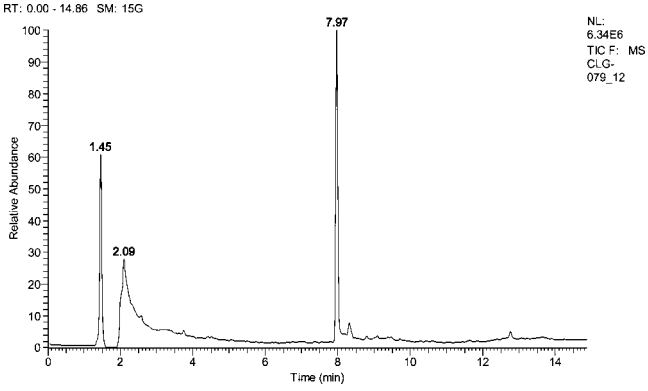

Figure 2. TIC of compound **5**, where compound t_R 1.45 min is CH_3SH, compound t_R 2.09 min is the residue CH_2Cl_2 reagent, and compound t_R 7.97 min is $(CH_2)5C{=}N{-}N{=}C{=}S$.

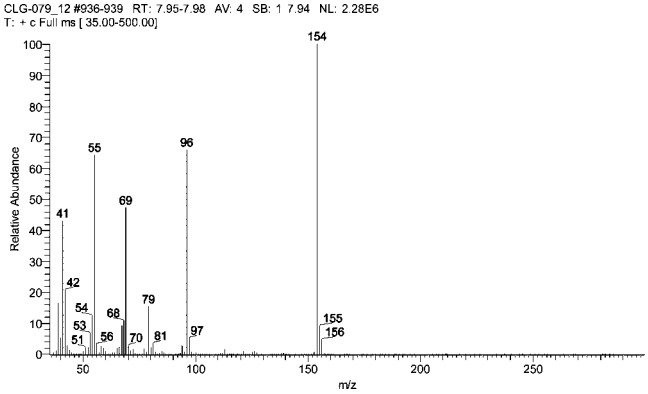

Figure 3. Mass spectra of the peak t_R 7.09 min in Figure 2.

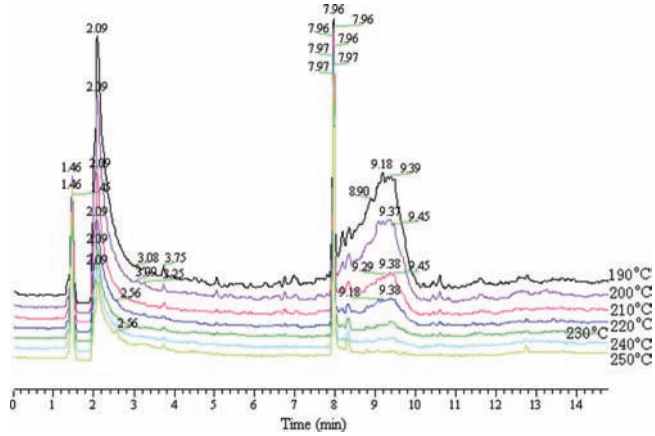

Figure 4. A series of TIC of compound **5** with different GC injector temperatures, where compound t_R 7.97 min and compound t_R 9.39 min are the same pyrolytic compound (*N*-isothiocyanatocyclohexanimine) formed in the heated injector and the capillary column, respectively.

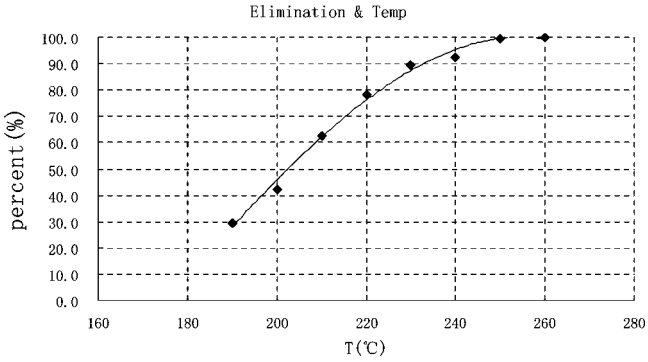

Figure 5. Plot of the pyrolitic efficiency in the GC injector versus its temperature for compound **5**.

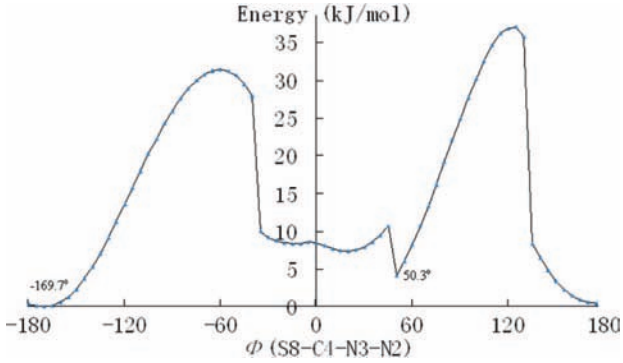

Figure 6. PM3 optimized rotational potential of compound **5** as a function of the Φ(S8−C4−N3−N2) dihedral angle.

With reducing the injector temperature, a decreasing portion of compound **5** undergoes pyrolysis in the GC injector, owing to the reduced reaction rate; and so an increasing quantity of the unreacted compound **5** vaporizes into the capillary column and then undergoes thermal decomposition. Therefore, as shown in Figure 4, the area of the peak t_R 7.97 min decreases and that of peak t_R 9.38 min increases with a reduction in the GC injector temperature, indicating that a decreasing proportion of the pyrolytic product was formed in the GC injector and an increasing proportion of the product was produced in the capillary column.

As shown in Figure 4, the peak t_R 9.38 min reaches the baseline of TIC, implying that the entire compound undergoes decomposition in the GC injector at a temperature of 250 °C. A plot of the pyrolytic efficiency in the GC injector versus its temperature was obtained as shown in Figure 5. The trend is clear. The pyrolytic rate decreases obviously when the temperature is reduced below 230 °C. Therefore, the GC injector must be set at a relatively high temperature to ensure that the analyte undergoes pyrolysis entirely in the injector for the GC and GC-MS determination of the thermolabile compounds.[3]

C. Molecular Structures of $R^1R^2C{=}N{-}NH{-}C(=S)SCH_3$. To interpret the above pyrolytic reaction, a conformational study of the five compounds in Chart 1 has been performed to obtain an idea of the minimum energy structures. Figure 6 describes the rotational potential $V(\Phi)$ of compound **5** obtained by varying the S8−C4−N3−N2 dihedral angle (Φ), using the semiempirical method PM3. Analysis of Figure 6 shows two configurational structures at the minimum energy by rotating the C4−N3 axis, with the dihedral angle (Φ) at −169.7° and 50.3°, respectively.

A full optimization of the two stable configurational structures has been carried out by using the PM3, B3LYP/6-31g(d), and B3LYP/6-31++g(2d,p) methods. Figure 7 shows the two equilibrium geometries (***syn*-Re** and ***trans*-Re**) of compound **5**. The characteristic difference of the two geometries is that H7 and the CH_3S- group are at the same side of the C4−N3 axis for ***syn*-Re**, and at the opposite side of the C4−N3 axis for ***trans*-Re**.

Parameters of the two optimized geometries are summarized in Table 2. In general, the semiempirical method PM3 only gave imprecise results, with much difference in geometrical parameters compared to the B3LYP/6-31g(d) method. However, geometrical parameters vary slightly as the basis set is expended from 6-31g(d) to 6-31++g(2d,p). The largest changes in bond lengths do not exceed 0.008 Å, and changes in valence angles and dihedral angles are also quite small—the largest change amounts to about 0.5°.

Analysis of Table 2 shows that the trans configuration of compound **5** (***trans*-Re**) has a nearly planar structure while the syn one (***syn*-Re**) is three-dimensional in its geometry. The r(N2−N3) bond length of ***trans*-Re** is about 0.057 Å shorter than that in ***syn*-Re** according to the calculation results by the DFT method, and the r(C4−S5) bond length of ***trans*-Re** is also about 0.026 Å shorter. The ∠(N2−N3−H7) bond angle is about 109° for ***syn*-Re** and 122° for ***trans*-Re**, respectively. Similar results at the 6-31g(d) level are obtained for the other four compounds in Chart 1 (see Table S1 in the Supporting Information). The above results indicate the sp^3 hybridization of N3 in the syn configurations, and sp^2 hybridization of N3 atom with the p−π conjugation of N3 with the C1═N2 double bond in the trans ones. The syn configuration of compound **1** shows an extra sp^2 hybridization of the N3 atom, owing to the conjugation of the phenyl group with the C1═N2 double bond, which promotes the p−π conjugation of N3 with the C1═N2 double bond.

***trans*-Re** is 26.9 kJ/mol lower in potential energy than ***syn*-Re** at the B3LYP/6-31++g(2d,p) theoretical level (as shown in Table 2), which decreases to 24.88 kJ/mol when free energies are considered. The above results show that the trans configuration is the more favorable structure in energy, owing to the conjugation of the lone electron pair on N3 with the C1═N2 double bond. Also, the other four compounds in Chart 1 exhibit similar results (see Table S1 in the Supporting Information).

The trans configuration and the syn one can also convert to each other through rotating the groups around the C4−N3 axis. For compound **5**, the barrier for conversion of ***syn*-Re** to ***trans*-Re** is about 50.67 kJ/mol, while in the reverse reaction it is 77.56 kJ/mol at the B3LYP/6-31++g (2d,p) theoretical level. The above results indicate that there is a preference for the trans configuration; however, the barrier is easy to overcome at the temperature of this study.

D. The Mechanisms of the Pyrolysis Reaction. The H7 atom on N3 in the structure of compounds **1**−**5** is an active hydrogen, and it transfers to S5 going with the breakage of the C4−S5 bond in the pyrolytic process, according to the pyrolytic products of these compounds. Such an hypothesis was verified by the compound dithiocarbamic amide, where the dithiocarbamic amide of primary amines can undergo decomposition while that of secondary amines (no active H within the molecule) does not.[3]

(1) Unimolecular Reaction Mechanism. In the unimolecular pyrolysis process, two leaving groups (H7 and CH_3S-) must be at the syn position to form a cyclic transition state.[1] Therefore, as shown in Scheme 2, ***syn*-Re** can undergo 1,2-elimination of CH_3SH and give the corresponding *N*-isothiocyanate imines in Path A. ***trans*-Re** can convert to ***syn*-Re** and continue to undergo pyrolysis through Path A. However, we postulate another

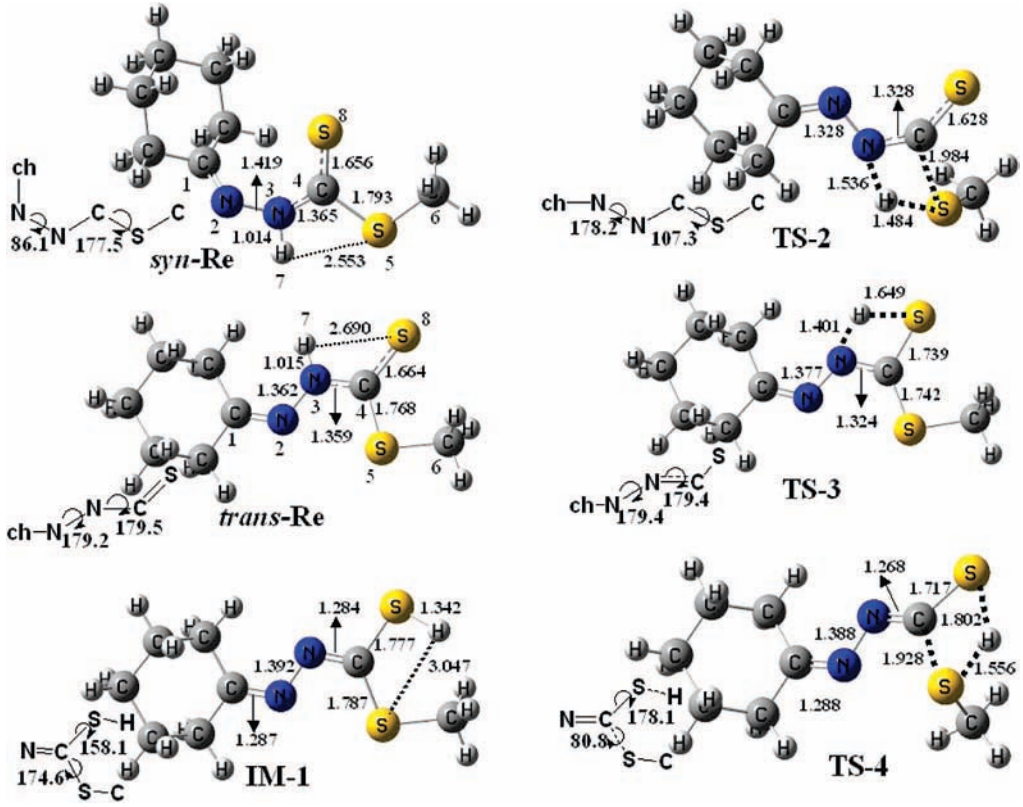

Figure 7. The B3LYP/6-31++g(2d,p) optimized structures of the key species in the unimolecular pyrolytic reactions of compound **5**.

TABLE 2: Selected Geometrical Parameters of Compound 5

	PM3		B3LYP/6-31G(d)		B3LYP/6-31++G(2d,p)	
coordinate[a]	syn	trans	syn	trans	syn	trans
r(C1−N2)	1.304	1.307	1.284	1.287	1.282	1.288
r(N2−N3)	1.394	1.392	1.424	1.364	1.419	1.362
r(N3−C4)	1.406	1.396	1.360	1.362	1.358	1.359
r(N3−H7)	1.006	1.006	1.016	1.017	1.014	1.015
r(C4−S5)	1.807	1.772	1.802	1.775	1.794	1.768
r(C4−S8)	1.604	1.639	1.660	1.667	1.657	1.665
r(S5−C6)	1.801	1.802	1.819	1.823	1.815	1.819
∠(C1−N2−N3)	121.7	121.6	116.3	120.2	116.8	119.1
∠(N2−N3−C4)	120.1	122.1	123.7	121.7	123.8	121.8
∠(N2−N3−H7)	115.7	117.7	109.4	122.5	109.7	122.4
∠(N3−C4−S5)	108.1	116.6	109.2	113.0	109.4	112.9
∠(N3−C4−S8)	127.7	118.1	125.9	120.3	125.8	120.2
∠(C4−S5−C6)	104.8	104.1	102.5	101.0	102.8	101.0
Φ(C1−N2−N3−C4)	−172.0	173.8	86.2	179.0	86.1	−179.1
Φ(N2−N3−C4−H7)	151.0	−161.1	140.2	178.7	177.0	178.2
Φ(H7−N3−C4−S5)	12.6	173.4	18.4	−179.4	0.6	−179.3
Φ(H7−N3−C4−S8)	−170.4	−8.6	−162.8	0.6	−179.7	0.9
Φ(N3−C4−S5−C6)	173.5	177.3	176.9	−179.80	178.59	−179.9
potential energy	7.5	0.0	29.7	0.0	26.9	0.0

[a] Bond lengths are in Å, angles in deg, and energies in kJ/mol. The energy *of* trans-compounds is taken to be zero.

reaction pathway for the thermal decomposition of ***trans*-Re** through Path B. Path B describes a two-step process, where H7 transfers to S8 and forms an intermediate of semidithioacetal (IM) in the first step, and then IM continues decomposition in the second step. To study the unimolecular pyrolysis of compound ketonic hydrazones from *S*-methyl dithiocarbazate according to the different reaction pathways in Scheme 2, compound **5** was selected as an example to interpret the above pyrolytic pathways.

***syn*-Re** undergoes a classical 1,2-elimination in Path A through a four-membered ring transition state (TS2), similar to pyrolysis of 1-furoyl-3-phenylthioureas.[14] The geometry of TS2 optimized at the B3LYP/6-31++G(2d,p) level is displayed in Figure 7. The normal vibrational mode that corresponds to the single imaginary frequency (−1040.3 cm^{-1}) is mainly related to the stretching of the N3−H7 bond that is breaking. By comparing with ***syn*-Re**, TS2 is found to have a much shorter S5−H7 distance (2.533 Å vs 1.484 Å), a much larger N3−H7 bond length (1.014 Å vs 1.536 Å), and a larger C4−S5 bond length (1.793 Å vs 1.984 Å). TS2 also shows a great twisting of the reactant, with a decreased ∠(C4−N3−H7) bond angle (116.0° vs 86.2°) and ∠(S5−C4−N3) bond angle (109.4° vs 95.3°). It is worth noting that the CH_3S group is twisted with regard to the dithiocarbazate moiety (N3−C4−S5−C6 dihedral

SCHEME 2: Proposed Mechanisms for the Unimolecular Pyrolysis of Compounds 1−5 in Chart 1

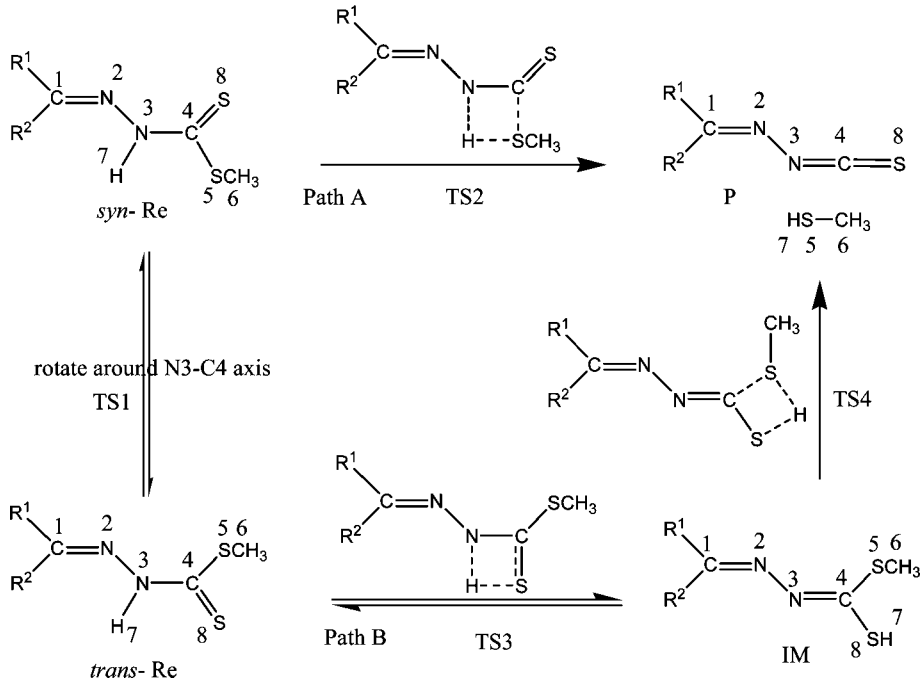

angle 105.7°), contrary to the situation in ***syn*-Re**, which has a planar arrangement. This twisting makes one of the lone electron pairs on the S6 face the active proton H7, and therefore favors the proton transfer. The above results indicate that the transfer of H7 from N3 to S5 and the breakage of the C4−S5 bond are taking place concertedly. An IRC calculation beginning at the TS2 shows that, when the forward direction is followed, the H7 atom is transferred to the S5 atom, and thus the ending products are confirmed as CH_3SH and $(CH_2)_5C{=}N{-}N{=}C{=}S$.

The first step reaction of Path B is described as a tautomer interconversion, where the H7 atom transfers to S8 and the double bond shifts from C4−S8 to N3−C4 through a four-membered ring transition state (TS3). As shown in Figure 7, the single imaginary frequency (-1561.8 cm^{-1}) of the optimized TS3 relates to the stretching of the N3−H7 bond that is breaking. In the structure of TS3, the bond H7−S8 (1.649 Å) is partially formed and the N3−H7 bond (1.401 Å) is essentially broken, compared to the corresponding bond length in ***trans*-Re**, which are 2.690 and 1.015 Å, respectively. Also, the ∠(C4−N3−H7) bond angle (82.2°) and the ∠(N3−C4−S8) bond angle (106.4°) are bent, with regard to the configuration of ***trans*-Re**, in which they are 115.7° and 120.3°, respectively. Completion of the tautomerization leads to a relative semidithioacetal compound (IM).

The 1,2-elimination of CH_3SH also occurs for IM in the second step of Path B, and yields $(CH_2)_5C{=}N{-}N{=}C{=}S$ through another four-membered ring transition state (TS4). The optimized structures of IM and TS4 are also exhibited in Figure 7. By comparing with IM, TS4 is found to have a much shorter S5−H7 distance (3.047 Å vs 1.556 Å), a much larger S8−H7 bond length (1.342 Å vs 1.802 Å), and a larger C4−S5 bond length (1.787 Å vs 1.928 Å). TS4 also shows a great twisting of IM, and a decreased ∠(C4−S8−H7) bond angle (98.1° vs 69.0°) and ∠(S5−C4−S8) bond angle (124.7° vs 104.2°). Similar to TS2, the twisting of the CH_3S group also occurs with regard to the semidithioacetal moiety in TS4 (N3−C4−S6−C7 dihedral angle 80.8°), which favors the proton transfer to S5. An IRC calculation beginning at the TS4 shows that, when the forward direction is followed, the H7 atom is transferred to the S5 atom to form CH_3SH and $(CH_2)_5C{=}N{-}N{=}C{=}S$, and IM is the end product in the backward direction.

A schematic potential and free energy surface for the two proposed reaction pathways is given in Figure 8. According to the energy of the reactants and the products, the decomposition is endothermic, with ΔE_A ($E_P - E_{syn\text{-}Re}$) being 21.95 kJ/mol for ***syn*-Re** and ΔE_B ($E_P - E_{trans\text{-}Re}$) being 48.48 kJ/mol for ***trans*-Re**. However, the free energies decrease by 3.17 kJ/mol during the pyrolytic process of ***trans*-Re** and 28.05 kJ/mol for that of ***syn*-Re**, and the decreasing values change to 45.75 and 69.0 kJ/mol, respectively, at the temperature (260 °C) of this study, indicating a spontaneous process of the pyrolysis reaction.

As shown in Figure 8, the activation energy (E_a) of the second step in Path B is 159.15 kJ/mol relative to that of ***trans*-Re**, which is 10.77 kJ/mol higher than that of the first step, indicating that the second step is the key step in Path B. However, Path A shows a higher barrier compared to the key step of Path B (E_a = 187.76 kJ/mol for Path A via E_a = 159.15 kJ/mol for Path B). Namely, computational results favor the two-step process by 28.61 kJ/mol. However, this difference is small and in the

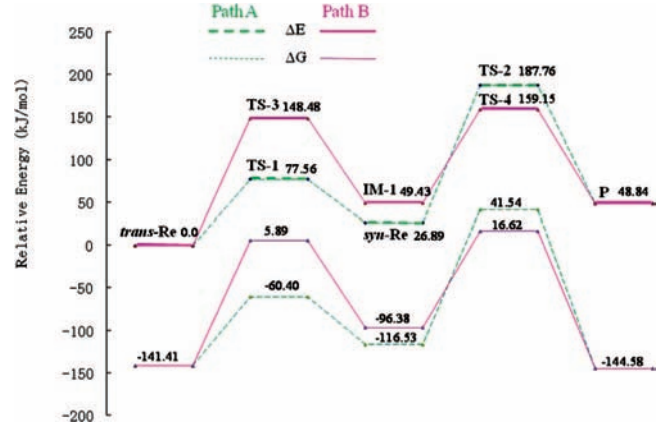

Figure 8. Potential and free energy reaction profile of the unimolecular reaction of compound **5**, calculated at the B3LYP/6-31++G(2d,p) level.

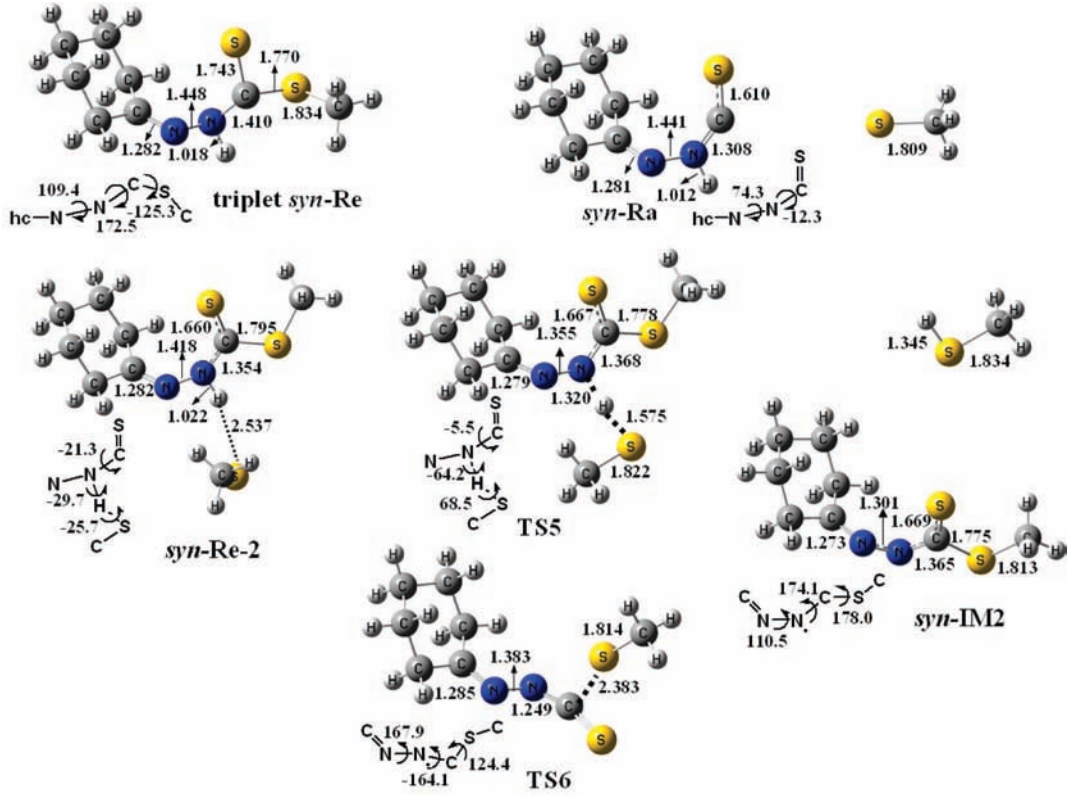

Figure 9. The geometries of species involved in the radical decomposition of *syn*-Re optimized at the uB3LYP/6-31++G(2d,p) level.

same amount of energy difference between the two configurations of the reactant (trans and syn), indicating that the two pyrolytic processes are viable provided that the pathway is intramolecular.

(2) The Free Radical Reaction Mechanism. In spin-allowed process of pyrolysis of compound **5**, both the syn and the trans configurations have their own vertical triplet excited state, **triplet *syn*-Re** and **triplet *trans*-Re**. The geometry of **triplet *syn*-Re** optimized at the uB3LYP/6-31++G(2d,p) level is displayed in Figure 9. As can be seen, the triplet excited character of **triplet *syn*-Re** is reflected in the lengthening of the N3−C4 bond from 1.365 Å to 1.410 Å and the C4−S8 bond from 1.656 Å to 1.743 Å, compared to ***syn*-Re** (Figure 7). It is worth noting that the dithiocarbazate moiety is nonplanar with the N3−C4−S8−S5 dihedral angle at −137.17°, contrary to the situation in ***syn*-Re**, which has a planar arrangement. The geometry of **triplet *trans*-Re** shows a similar triplet excited character to **triplet *syn*-Re**, with stretching the N3−C4 bond and the C4−S8 bond and twisting the dithiocarbazate moiety (see Figure S4 in the Supporting Information). The above results show that one electron in the C4−S8 double bond is excited into the antibonding molecule orbit in the triplet excited structures. The residue lone electron triggers the hemolytic breakage of the C4−S5 bond and yields two radicals, the methylthiol radical **MeS$^{\bullet}$** and the radical ***syn*-Ra** or ***trans*-Ra**. The above process is the initiation step of the free radical pyrolysis of compound **5**.

A schematic potential and free energy surface for the initiation step of the radical pyrolysis is given in Figure 10. As can be seen, **triplet *trans*-Re** is 253.60 kJ/mol higher in potential energy than its ground state ***trans*-Re**, and it decreases to 244.92 kJ/mol when free energies are considered. The free energy decreases by 31.19 kJ/mol in the decomposition process of **triplet *trans*-Re**, although there is an increase in the potential energy. In terms of **triplet *syn*-Re**, it locates 235.14 kJ/mol

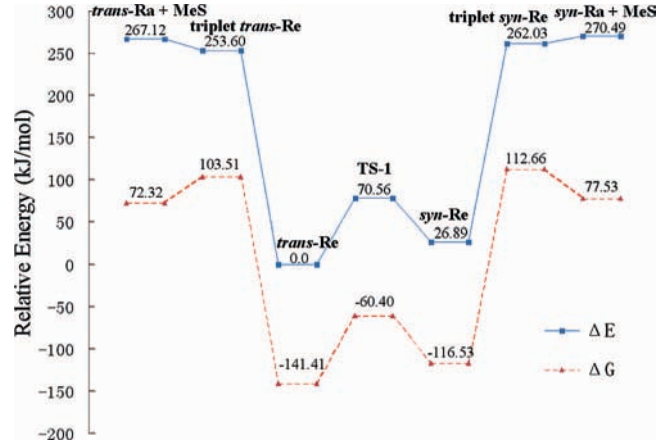

Figure 10. Potential and free energy reaction profile of the initiation step of the radical pyrolysis of compound **5**, calculated at the uB3LYP/6-31++G(2d,p) level.

above its ground state in the potential energy, and it decreases to 229.19 kJ/mol when free energies are considered. The variation in energies during the decomposition of **triplet *syn*-Re** is similar to that of **triplet *trans*-Re**. However, **triplet *syn*-Re** and its pyrolytic products show 8.43 and 3.27 kJ/mol higher in potential energy than **triplet *trans*-Re** and its pyrolytic products, respectively. And they increase to 9.11 and 5.21 kJ/mol, respectively, when free energies are considered. Namely, decomposition of **triplet *trans*-Re** is slightly more favorable in energies than that of **triplet *syn*-Re** in the initiation step of the radical pyrolysis.

According to the pyrolytic products, the propagation step in the radical decomposition of ***syn*-Re** is postulated in Scheme 3. The methylthio radical **MeS$^{\bullet}$**, which is formed by decomposition of **triplet *syn*-Re**, captures the active hydrogen on N3 of ***syn*-Re**, and yields methanethiol and another radical ***syn*-IM2**

SCHEME 3: Proposed Mechanisms for the Radical Pyrolysis of *syn*-Re of Compound 5

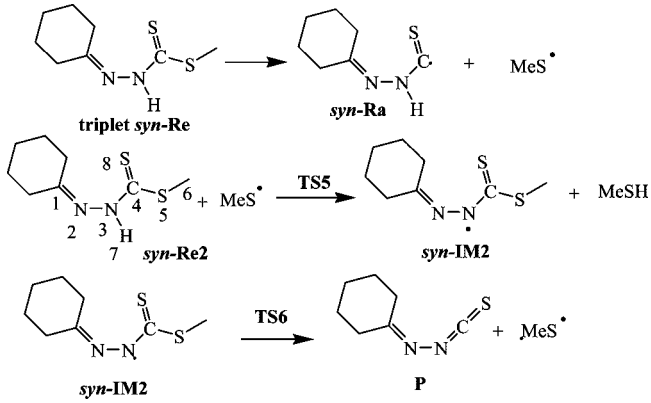

via transition state **TS5**. ***syn*-IM2** continues to undergo fragmentation and gives pyrolytic product **P** (*N*-isothiocyanate cyclohexanimine) and another particle of methylthio radical **MeS•** through transition state **TS6**, and the produced methylthio radical will trigger another pyrolytic reaction. The geometries of species involved in the radical decomposition of ***syn*-Re** optimized at the uB3LYP/6-31++G(2d,p) level are displayed in Figure 9.

The optimized structure of **TS5** corresponds to a situation in which the proton from the N3−H7 group is being transferred to the methylthio radical. By comparing to ***syn*-Re**, the transfer of proton in **TS5** is reflected in the lengthening of the N3−H8 bond from 1.022 Å to 1.320 Å, and the shrinking of the H8−SMe distance from 2.513 Å to 1.575 Å. The vibrational mode of the single imaginary frequency (−1633.9 cm^{-1}) is mainly related to the stretching of the N3−H7 bond that is breaking. The completion of hydrogen transfer leads to methanethiol and the radical ***syn*-IM2**. The geometry of ***syn*-IM2** is very similar to that of ***syn*-Re**, except for a remarkable shrinkage in the N2−N3 bond length (1.419 Å vs 1.301 Å).

The transition state (**TS6**) for decomposition of ***syn*-IM2** shows a breaking C4−S5 bond with the distance at 2.383 Å and a twisting arrangement of the methylthio group with regard to the thiocarbenic moiety with the N3−C4−S5−C6 dihedral angle at 124.4°. Geometrical parameters show the losing methylthio radical compared to ***syn*-IM2** as exhibited in the lengthening of the N2−N3 bond from 1.301 Å to 1.383 Å, in the shrinking of the N3−C4 bond from 1.365 Å to 1.249 Å, and in the enlarging of the N3−C4−S8 bond angle from 126.9° to 156.2°. Completion of the decomposition leads to *N*-isothiocyanate cyclohexanimine (**P**) and another particle of methylthio radical (**MeS•**).

The propagation step in the radical decomposition of ***trans*-Re** is also similar to that of ***syn*-Re**, with some differences in the degree of reaction (see Scheme S1 and Figure S4 in the Supporting Information). For example, a reducing distance of H7-•**SMe** from 2.537 Å to 2.274 Å is found in ***trans*-Re2**, showing a hydrogen bond in the complex of methylthio radical and ***trans*-Re**, relative to ***syn*-Re2** (the complex of methylthio radical and ***syn*-Re**). In the process of proton transfer, H7 on N3 is transferred to a greater extent to the methylthio radical in **TS7** than in **TS5**, with longer N3−H7 distance (1.320 Å vs 1.582 Å) and shorter H7-•**SMe** distance (1.575 Å vs 1.453 Å). Also, a greater extent of the decomposition is found in ***trans*-IM2** than in ***syn*-IM2**, evidenced by the longer C4−S5 distance in **TS8** compared to **TS6** (2.383 Å vs 2.471 Å). These different reaction degrees are exhibited in the differences in the energy profiles of the pyrolytic reactions.

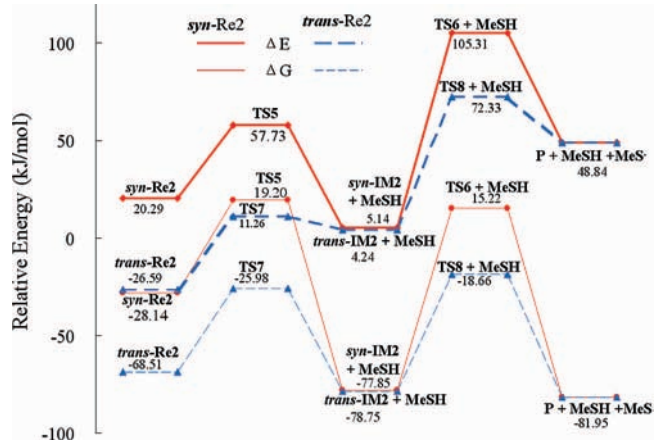

Figure 11. Potential and free energy reaction profile in the propagation step of the radical pyrolysis of compound **5**, calculated at the uB3LYP/6-31++G(2d,p) level.

Figure 11 shows the potential and free energy reaction profiles at the uB3LYP/6-31++G(2d,p) theoretical level in the propagation step of the radical pyrolysis of compound **5**. It should be pointed out that the sum potential energy of ***trans*-Re** and the methylthio radical is set to zero. Owing to the hydrogen bond between H8 and the methylthio radical (**MeS•**), the potential energy of ***trans*-Re2** decreases to −26.59 kJ/mol, which is 48.88 kJ/mol lower than that of ***syn*-Re2**.

In the radical pyrolysis of ***trans*-Re**, the calculated activation energy is 37.85 kJ/mol relative to ***trans*-Re2** in the first step (**TS5**, hydrogen transfer) of the propagation process, and it increases to 42.53 kJ/mol when free energies are considered. The activation energy for the second step (**TS6**, breakage of the C4−S5 bond) is 68.09 kJ/mol, and it increases to 98.92 kJ/mol relative to ***trans*-Re2**, and then changes to 59.49 and 49.85 kJ/mol, respectively, when free energies are considered. The above results indicate that the second step is the rate-determining step in the propagation step of the radical pyrolysis.

In terms of the radical pyrolysis of ***syn*-Re**, similar results are obtained by analysis of Figure 11, showing that the second step (**TS8**, breakage of the C4−S5 bond) is also the rate-determining step in the radical propagation process. The activation energy for the critical step (**TS8**) is 131.91 kJ/mol relative to ***trans*-Re2**, which is 32.98 kJ/mol higher than that in the radical pyrolysis of ***trans*-Re**. Namely, the radical pyrolysis of compound **5** favors the decomposition of ***trans*-Re** slightly, by comparing with the energy barriers of the two valid processes.

Comparing with the unimolecular pyrolysis of compound 5, both ***syn*-Re** and ***trans*-Re** exhibit lower critical energies in the propagation step of the radical pyrolysis (187.76 kJ/mol vs 131.91 kJ/mol for pyrolysis of ***syn*-Re**, and 159.15 kJ/mol vs 98.92 kJ/mol for pyrolysis of ***trans*-Re**). However, much more energy is needed to excite the compound to produce radical in the initiation step of the radical pyrolysis, with 262.03 and 253.60 kJ/mol for ***syn*-Re** and ***trans*-Re**, respectively. Therefore, the radical pyrolysis is a more favorable process provided the radical initiator is present, whereas the unimolecular pyrolysis mechanism rather than the radical pyrolysis one occurs in the pyrolytic process of compound **5** in the condition of this study, according to the theoretical calculations.

Conclusions

The present study reports the gas phase pyrolytic eliminations of ketonic hydrazones from *S*-methyl dithiocarbazate

$R_1(R_2)C{=}N{-}NHC(=S)SCH_3$ (R_1, R_2 = alkyl or aryl) by online pyrolysis on GC-MS and theoretical calculation.

The experimental results show that the EI mass spectra of the above compounds could be obtained only by direct sample introduction, whereas they underwent online pyrolysis to produce CH_3SH and $R_1(R_2)C{=}N{-}N{=}C{=}S$ when analyzed by GC-MS. The GC-MS experiments of cyclohexanonic hydrazone from *S*-methyl dithiocarbazate (compound **5**) show that the pyrolysis occurred in both the GC injector and the capillary column, and gave two peaks with the same prolytic product (*N*-isothiocyanate cyclohexanimine) in the TIC. With reducing the GC injector temperature, a decreasing portion of compound **5** underwent pyrolysis in the injector and an increasing quantity of the unreacted compound vaporized into the capillary column for thermal decomposition.

Theoretical calculations also show two stable configurational structures with H7 on the N atom and the CH_3S- group at the same side and the opposite side relative to the N3−C4 axis (***syn*-Re** and ***trans*-Re**). ***trans*-Re** is thermodynamically more stable than ***syn*-Re**, and they can convert to each other by rotating the N3−C4 axis. Both the unimolecular and the radical mechanisms were postulated and studied for pyrolysis of compound **5** by the DFT theoretical method.

In the unimolecular pyrolytic process, ***syn*-Re** directly undergoes 1,2-elimination to yield methanethiol and *N*-isothiocyanate cyclohexanimine (Path A), while ***trans*-Re** undergoes tautomer conversion and leads to an intermediate of semidithioacetal (**IM**) followed by 1,2-elimination of CH_3SH (Path B). A schematic potential energy surface shows that the decomposition is spontaneous and the pyrolytic mechanism prefers Path B, although the two pyrolytic processes are viable.

In terms of the radical pyrolysis, both ***trans*-Re** and ***syn*-Re** react with the methylthio radical, which is produced by fragment of the excited state of compound **5**, involving a two-step process, proton transfer and the breakage of the C−S bond. The second step (the breakage of the C−S bond) is the rate-determining step in the propagation process of the radical decomposition, and the radical pyrolysis of ***trans*-Re** is also slightly more favored thermodynamically than that of ***syn*-Re**.

Theoretical calculations also show that both ***syn*-Re** and ***trans*-Re** have lower critical energies in the propagation step of the radical pyrolysis than in the unimolecular pyrolysis process, whereas much more energy is needed to excite the compound to produce the methylthio radical in the initiation step of the radical pyrolysis. Therefore, the unimolecular pyrolysis mechanism rather than the radical pyrolysis occurs in the pyrolytic process of compound **5** in the condition of this study.

This theoretical study is, however, limited to a description of the lowest potential energy surface in both unimolecular and radical pyrolysis of cyclohexanonic hydrazones from *S*-methyl dithiocarbazate at the B3LYP/6-31++g(2d,p) level.

Acknowledgment. The authors gratefully acknowledge the financial support from Ministry of Education of China (NCET-06-0520) and NSF of Zhejiang Province (Z2006510).

Supporting Information Available: Scheme S1 gives the proposed mechanisms for the radical pyrolysis of ***trans*-Re** (compound **5**); Table S1 gives selected geometrical parameters of compounds **1**−**5**, optimized at the B3LYP/6-31 g(d) level; Figure S1 gives the EI-MS of compounds **1**−**5** in Table 1 (from up to down) by the direct introduction method; Figure S2 gives the EI-MS of the pyrolytic products corresponding to compounds **1**−**5** in Table 1 (from up to down) by online GC-MS pyrolysis; Figure S3 gives mass spectra of the peak t_R 7.96 min and the peak t_R 9.83 min in Figure 4, ascribed to the same compound (*N*-isothiocyanatecyclohexanimine); Figure S4 gives the geometries of species involved in the radical decomposition of ***trans*-Re** optimized at the uB3LYP/6-31++G(2d,p) level; and geometries, total energies, and zero-point energy corrections for ***syn*-Re**, ***trans*-Re**, **TS1**, **TS2**, **P1**: $(CH_2)_5C{=}N{-}NCS$, **P2**: CH_3SH, **TS3**, **IM**, **TS4**, **triplet *syn*-Re**, **MeS$^\bullet$**, ***syn*-Ra**, ***syn*-Re2**, **TS5**, ***syn*-IM2**, **TS6**, **triplet *trans*-Re**, ***trans*-Ra**, ***trans*-Re2**, **TS7**, ***trans*-IM2**, **TS8**. This material is available free of charge via the Internet at http://pubs.acs.org.

References and Notes

(1) Smith, M. B.; March, J. *March's Advanced Organic chemistry (Reactions, Mechanisms and Structure)*, 5th ed.; Wiley: New York, 2001; Chapter 17.

(2) (a) Tsuge, S.; Yokoi, H.; Ishida, Y.; Ohtani, H.; Becker, M. A. *Polym. Degrad. Stab.* **2000**, *69*, 223–227.

(3) (a) Grzegorz, B.; Jozef, K.; Edmund, M.; Janusz, S. *J. Chromatogr.* **1980**, *193* (1), 61–69. (b) Gaind, V. S.; Chai, F. *Analyst* **1990**, *115*, 143–145. (c) Vandana, S.; Manju, G.; Archana, J.; Krishna, K. V. *J. Chromatogr. A* **2003**, *1010*, 243–253.

(4) Johnson, M. R. *J. Org. Chem.;* **1986**, *51* (6), 833–837.

(5) Jenneskens, L. W.; Hoefs, C. A. M.; Wiersum, U. E. *J. Org. Chem.* **1989**, *54*, 5811–5814.

(6) Lane, T. J.; Sam, A.; Kandathil, A. J. *J. Am. Chem. Soc.* **1960**, *82*, 4462–4464.

(7) Higgins, C. E.; Baldwin., W. H. *J. Org. Chem.* **1965**, *30* (9), 3173–3176.

(8) Arnold, R. T.; Smolinsky, C. *J. Org. Chem.* **1960**, *25*, 129–130.

(9) (a) Barton, D. H. R.; Howlett, K. E. *J. Chem. Soc.* **1949**, *155*, 165.

(10) Yang, B.; Tian, S.; Zhao, S. *Fuel Process. Technol.* **2006**, *87*, 673–678.

(11) (a) Rummens, F. H. A. *Recl. Trav. Chim. Pays-Bas* **1964**, *83*, 901. (b) Louw, R.; Kooyman, E. C. *Recl. Trav. Chim. Pays-Bas* **1965**, *84*, 1151.

(12) Chen, L. Z.; Bian, G. F.; Jiang, K. Z.; Wu, J. R.; Lai, G. Q. *ACTA Chim. Sin. (Chin. Ed.)* **2007**, *65* (17), 1897–1901.

(13) (a) Pedersen, C. Th.; Bech, A. T.; Flammang, R.; Wentrup, C. *Phosphorus, Sulfur Silicon Relat. Elem.* **1999**, *153*−*154*, 329–330. (b) Pedersen, C. Th.; Flammang, R. *Phosphorus, Sulfur Silicon Relat. Elem.* **2005**, *180* (5−6), 1395–1398.

(14) Macias, A.; Rosado, A.; Otazo, E. *J. Anal. Appl. Pyrolysis* **1996**, *38*, 55–60.

(15) Atalla, A. A.; Kamal Ei-Dean, A. M.; Gaber, A. M. *Phosphorus, Sulfur Silicon Relat. Elem.* **1996**, *117*, 205–212.

(16) (a) Chuchani, G.; Pekerar, S.; Dominguez, R. M.; Rotinov, A.; Martin, I. *J. Phys. Chem.* **1989**, *93* (1), 201–202. (b) Chuchani, G.; Domhguez, R. M.; Rotinov, A.; Mardn, I. *J. Phys. Chem.* **1989**, *93*, 206–208. (c) Chuchani, G.; Domhguez, R. M.; Rotinov, A.; Mardn, I. *J. Phys. Chem.* **1990**, *94*, 3341–3343.

(17) (a) Cordeiro, M. N. D. S.; Dias, A. A.; Costa, M. L.; Gome, J. A. N. F. *J. Phys. Chem. A* **2001**, *105*, 3140–3147. (b) Ge, Y.; Gordon, M.; Battaglia, S. F.; Fox, R. O. *J. Phys. Chem. A.* **2007**, *111*, 1475–1486. (c) Kalra, B. L.; Lewis, D. K.; Singer, S. R.; Raghavan, A. S.; Baldwin, J. E.; Hess, B. A., Jr. *J. Phys. Chem. A* **2004**, *108* (52), 11554–11558. (d) Chen, S. C.; Xu, S. C.; Diau, E.; Lin, M. C. *J. Phys. Chem. A* **2006**, *110* (33), 10130–10134.

(18) Lee, I.; Cha, O. J.; Lee, B. S. *J. Phys. Chem.* **1990**, *94*, 3926–3930.

(19) Carcía, J. I.; Hummeres, E. *J. Org. Chem.* **2002**, *67*, 2755–2761.

(20) Lu, A. M.; Ding, W. J.; Liu, R. Z. *J. Beijing Norm. Univ., Nat. Sci.* **2006**, *42*, 287–290.

(21) Klayman, D. L.; Bartosevich, J. F.; Griffin, T. S.; Mason, C. J.; Scovill, J. P. *J. Med. Chem.* **1979**, *22*, 7855–862.

(22) (a) Sengupta, S. K.; Kumar, S. *Synth. React. Inorg. Met.-Org. Chem.* **1982**, *12* (3), 297–307. (b) Chinnusamy, V.; Muthusamy, G.; Natarajan, K. *Synth. React. Inorg. Met.-Org. Chem.* **1994**, *24* (4), 561–74. (c) Abdelhamid, A. O.; El-Ghandour, A. H.; Hussein, A. M.; Zaki, Y. H. *J. Sulfur Chem.* **2004**, *25* (5), 329–342.

(23) (a) *DSQ Mass Spectrometer User Manuals*; Thermo Fisher Scientific: Austin, TX, 2003. (b) Natail, N.; Chinnici, F.; Riponi, C. *J. Agric. Food Chem.* **2006**, *54* (21), 8190–8198. (c) Pongsuwan, W.; Bamba, T.; Yonetani, T.; Kobayashi, A.; Fukusaki, E. *J. Agric. Food Chem.* **2008**, *56* (3), 744–750. (d) Peter, S.; Spiteller, P. *J. Nat. Prod.* **2006**, *69* (12), 1809–1812.

(24) Frisch, M. J.; Trucks, G. W.; Schlegel, H. B.; Scuseria, G. E.; Robb, M. A.; Cheeseman, J. R.; Zakrzewski, V. G.; Montgomery, J. A., Jr.; Stratmann, R. E.; Burant, J. C.; Dapprich, S.; Millam, J. M.; Daniels, A. D.; Kudin, K. N.; Strain, M. C.; Farkas, O.; Tomasi, J.; Barone, V.; Cossi, M.; Cammi, R.; Mennucci, B.; Pomelli, C.; Adamo, C.; Clifford, S.; Ochterski,

J.; Petersson, G. A.; Ayala, P. Y.; Cui, Q.; Morokuma, K.; Malick, D. K.; Rabuck, A. D.; Raghavachari, K.; Foresman, J. B.; Cioslowski, J.; Ortiz, J. V.; Stefanov, B. B.; Liu, G.; Liashenko, A.; Piskorz, P.; Komaromi, I.; Gomperts, R.; Martin, R. L.; Fox, D. J.; Keith, T.; AlLaham, M. A.; Peng, C. Y.; Nanayakkara, A.; Gonzalez, C.; Challacombe, M.; Gill, P. M. W.; Johnson, B.; Chen, W.; Wong, M. W.; Andres, J. L.; Gonzalez, C.; HeadGordon, M. E.; Replogle, S.; Pople, J. A. *Gaussian03*; Gaussian Inc., Pittsburgh, PA, 2003.

(25) Bauschlicher, C. W., Jr. *Chem. Phys. Lett.* **1995**, *246*, 40–44.

JP808273M